A Computational Comparison of two FEM Solvers For Nonlinear Incompressible Flow

J. Hron, A. Ouazzi, and S. Turek

Institute of Applied Mathematics, University of Dortmund,
Vogelpothsweg 87, 44227 Dortmund, Germany

Abstract. In this comparative study, we examine the influence of two different FEM discretization techniques (conforming Q_2/P_1, nonconforming $\tilde{Q}_1/Q_0$ Stokes element) and solution procedures (nonlinear Newton variants and multigrid vs. Krylov-space solvers for the linear subproblems) onto the approximation properties and particularly the total efficiency of corresponding CFD simulation tools. We discuss algorithmic details and give numerical results for laminar incompressible flow examples including non-Newtonian behavior of *power law* type.

1 Introduction

The finite element pair Q_2/P_1, being potentially of 3rd order accuracy due to the biquadratic polynomials for the velocity (and the linear pressure approximation), is one of the most popular discretization techniques in the CFD community. In most applications, it is employed in a fully coupled approach which applies an outer Newton-like iteration for the discretized Navier-Stokes equations while the resulting linear subproblems of Oseen-type (as a non-symmetric generalization of Stokes problems) are treated with (single-grid) Krylov-space methods: Due to the indefinite and particularly non-symmetric character of the equations, preconditioned BiCGSTAB [17] and GMRES [10] variants are the most popular solvers for the corresponding linear systems.

As an alternative, see for instance the realization in the FEATFLOW software package [15], special nonconforming FEM elements like the rotated multilinear/piecewise constant $\tilde{Q}_1/Q_0$ Stokes element have been developed which provide an optimal approximation error of one order less. However, for such finite elements, special hierarchical multigrid techniques have been successfully realized.

AS a consequence, such 'linear' (low order) finite elements seem to require much more degrees of freedom to satisfy a prescribed accuracy than compared with the quadratic Q_2/P_1 ansatz, while they show at the same time a much superior behavior w.r.t. the efficiency of the involved solvers. Therefore, the aim of this paper is to analyze the numerical characteristics of both popular approaches and to give an absolute comparison for non-trivial flow configurations in 2D which are based on the (nonlinear) incompressible Navier-Stokes equations:

'What is the total efficiency in terms of CPU timing, if we take into account the different numbers of unknowns and iteration steps which are required for a comparatively accurate simulation?'

The paper is organized as follow: In section §2 we present the problem formulations, while in §3 the two Stokes elements, the conforming Q_2/P_1 element pair and the stabilized version of the rotated bilinear $\tilde{Q}_1/Q_0$ Stokes element for problems involving deformation tensor formulation, are introduced. Two Newton linearization techniques, based on a continuous approach which first calculates the continuous Jacobi matrix and then performs the FEM discretization, in contrast to a discrete variant based on 'divided differences' for the discretized nonlinear stiffness matrices, are developed in §4. A brief description of the employed linear solvers, namely preconditioned GMRES and a local 'multilevel pressure Schur complement' smoother of so-called Vanka-type inside of a direct multigrid approach are presented in §5. Finally, section §6 is devoted to a discussion of algorithmic details and to show numerical results for different flow configurations which all are related to the standard 'Flow around cylinder' CFD benchmark [12].

2 Problem Formulation

In the underlying Navier-Stokes problem, the Cauchy stress tensor is given by $\boldsymbol{\sigma} = 2\nu(D_{\mathrm{II}}(\boldsymbol{u}))\mathbf{D}(\boldsymbol{u}) - p\mathbf{I}$, where p is the pressure; $\mathbf{D}(\boldsymbol{u}) = \frac{1}{2}(\nabla\boldsymbol{u} + \nabla^T\boldsymbol{u})$ is the rate of deformation tensor, $\boldsymbol{u}$ being the velocity; $\nu(\cdot)$ is the viscosity which can depend on the second invariant of the rate deformation tensor $D_{\mathrm{II}}(\boldsymbol{u}) = \frac{1}{2}\operatorname{tr}(\mathbf{D}^2(\boldsymbol{u}))$. Then, depending on the chosen viscosity function, the following prototypical models are used in certain applications (with appropriate parameters $\nu_0, \nu_\infty, \lambda, \alpha$):

- 'power law' defined for $\nu(z) = \nu_0 z^{\frac{\alpha}{2}}$
- 'Carreau law' defined for $\nu(z) = \nu_\infty + (\nu_0 - \nu_\infty)(1 + \lambda z)^{\frac{\alpha}{2}}$
- 'Bingham law' defined for $\nu(z) = z^{-\frac{1}{2}}$

In the following, we will mainly concentrate on the 'power law' model with varying parameter α. Moreover, we recently performed similar tests for models with a pressure-dependent viscosity [7, 5], as for instance the 'Schaeffer law' [11] with $\nu(z) = pz^{-\frac{1}{2}}$ which is a special model for granular flow.

Altogether, the velocity $\boldsymbol{u}$ and the pressure p satisfy the following generalized incompressible Navier-Stokes equations:

$$\frac{\partial \boldsymbol{u}}{\partial t} + \boldsymbol{u}\cdot\nabla\boldsymbol{u} - \operatorname{div}\left(2\nu(D_{\mathrm{II}}(\boldsymbol{u}))\mathbf{D}(\boldsymbol{u})\right) + \nabla p = \boldsymbol{f}, \quad \operatorname{div}\boldsymbol{u} = 0 \tag{1}$$

Let us consider a stationary flow governed by the generalized Navier-Stokes problem (1) in a bounded domain $\Omega \subset \mathbb{R}^2$. If we restrict the set V of

test functions to be divergence-free and if we take the constitutive laws into account, the above equations (1) lead to:

$$\int_\Omega 2\nu(D_{\mathrm{II}}(\boldsymbol{u}))\mathbf{D}(\boldsymbol{u}) : \mathbf{D}(\boldsymbol{v})\,dx + \int_\Omega (\boldsymbol{u}\cdot\nabla\boldsymbol{u})\boldsymbol{v}\,dx = \int_\Omega \boldsymbol{f}\boldsymbol{v}\,dx,\ \forall \boldsymbol{v}\in V \quad (2)$$

Some existence and uniqueness statements for (2) are given in [1], [8]. It is straightforward to penalize the constraint $\operatorname{div}\boldsymbol{v}=0$ to derive the equivalent mixed formulations of (2):

Find $(\boldsymbol{u},p)\in X\times M$ such that

$$\begin{aligned}\int_\Omega 2\nu(D_{\mathrm{II}}(\boldsymbol{u}))\mathbf{D}(\boldsymbol{u}) : \mathbf{D}(\boldsymbol{v})\,dx + \int_\Omega (\boldsymbol{u}\cdot\nabla\boldsymbol{u})\boldsymbol{v}\,dx \quad &+\int_\Omega p\operatorname{div}\boldsymbol{v}\,dx \\ = \int_\Omega \boldsymbol{f}\boldsymbol{v}\,dx, \qquad &\forall \boldsymbol{v}\in X, \\ \int_\Omega q\operatorname{div}\boldsymbol{u}\,dx = 0, \qquad &\forall q\in M,\end{aligned} \quad (3)$$

with the spaces $X=\mathbf{H}_0^1(\Omega)$ and $M=L_0^2(\Omega)$. For the following considerations, we introduce the bilinear forms:

$$\langle \mathbf{A}(\boldsymbol{w})\boldsymbol{u},\boldsymbol{v}\rangle = \int_\Omega 2\nu(D_{\mathrm{II}}(\boldsymbol{w}))\mathbf{D}(\boldsymbol{u}) : \mathbf{D}(\boldsymbol{v})\,dx \quad (4)$$

$$\langle \mathbf{N}(\boldsymbol{w})\boldsymbol{u},\boldsymbol{v}\rangle = \int_\Omega (\boldsymbol{w}\cdot\nabla\boldsymbol{u})\boldsymbol{v}\,dx \quad (5)$$

$$\langle \mathbf{B}q,\boldsymbol{v}\rangle = \int_\Omega q\operatorname{div}\boldsymbol{v}\,dx \quad (6)$$

Then, we can rewrite our generalized flow problems in the following more compact form:

Find $(\boldsymbol{u},p)\in X\times M$ such that

$$\begin{aligned}\langle \mathbf{A}(\boldsymbol{u})\boldsymbol{u},\boldsymbol{v}\rangle + \langle \mathbf{N}(\boldsymbol{u})\boldsymbol{u},\boldsymbol{v}\rangle + \langle \mathbf{B}p,\boldsymbol{v}\rangle = \int_\Omega \boldsymbol{f}\boldsymbol{v}\,dx, \quad &\forall \boldsymbol{v}\in X, \\ \langle \mathbf{B}q,\boldsymbol{u}\rangle = 0, \qquad &\forall q\in M.\end{aligned} \quad (7)$$

3 Discretization Aspects

3.1 The conforming Stokes Element Q_2/P_1

We discretize the continuous problem (3) by the standard Galerkin finite element method, hereby approximating the Ω by a domain Ω_h with piecewise linear boundary which is equipped with a quadrilateral mesh $\mathcal{T}_h$. On this mesh

we define the finite dimensional spaces V_h and P_h for the velocity and the pressure approximations as

$$V_h = \{\boldsymbol{v}_h \in \mathbf{H}_0^1(\Omega_h)^2, \quad \boldsymbol{v}_{h|T} \in Q_2(T)^2 \ \ \forall T \in \mathcal{T}_h, \quad \boldsymbol{v}_h = \mathbf{0} \text{ on } \partial\Omega_h\}, \quad (8)$$

$$P_h = \{p_h \in L^2(\Omega_h), \quad p_{h|T} \in P_1(T) \ \ \forall T \in \mathcal{T}_h\}. \quad (9)$$

By $Q_2(T)$ we denote the standard biquadratic space on the quadrilateral T which, when transformed by the bilinear transformation to the reference quadrilateral $T_{\text{ref}} = (-1, 1)^2$, is defined by

$$Q_2(T_{\text{ref}}) = \text{span}\{1, \xi, \eta, \xi\eta, \xi^2, \eta^2, \xi^2\eta, \xi\eta^2, \xi^2\eta^2\}, \quad (10)$$

with the 9 local degrees of freedom located at the vertices, midpoints of the edges and in the center of the quadrilateral. The space $P_1(T)$ consists of linear functions defined on the reference element by

$$P_1(T_{\text{ref}}) = \text{span}\{1, \xi, \eta\}, \quad (11)$$

with the function value and both partial derivatives in the center of the quadrilateral as its 3 local degrees of freedom. Recently, we modified the ansatz via using a non-parametric version for $P_1(T)$ working without transformation to the reference element.

For smooth solutions, the approximation error for the velocity in the L^2-norm is of order $O(h^3)$ which can be easily demonstrated for prescribed polynomials or for smooth data on appropriate domains. However, the actual approximation properties for local quantities as drag and lift coefficient, for instance on the surface of objects in the flow field, is not so clear. And, it is by far not obvious what to do in the case of moderate or even high Reynolds numbers: Due to the dominance of the convective term, certain stabilization techniques like FEM upwinding or streamline-diffusion are non-trivial to construct, and the resulting approximation properties, particularly for realistic flow configurations, is not clear. Therefore, we will follow the 'standard approach' for this Stokes element, namely performing pure central differencing - which is the shown Galerkin discretization without any additional stabilization. Since the discussed flow configurations are in the low Reynolds number regime, this approach is justified. However, the reader should keep in mind that the extension of our results to higher Reynolds numbers is not clear at all.

3.2 The nonconforming Stokes Element $\tilde{Q}_1/Q_0$

Again, we consider a subdivision $T \in \mathcal{T}_h$ consisting of quadrilaterals in the domain $\Omega_h \in \mathbb{R}^2$, and we employ the rotated bilinear *Rannacher-Turek* element [9]. For any quadrilateral T, let (ξ, η) denote a local coordinate system

obtained by joining the midpoints of the opposing faces of T. Then, in the *non-parametric* case, we set on each element T

$$\tilde{Q}_1(T) := \text{span}\left\{1, \xi, \eta, \xi^2 - \eta^2\right\}. \tag{12}$$

The degrees of freedom are determined by the following nodal functionals $\{F_\Gamma^{(a,b)}(\cdot), \Gamma \subset \partial\mathcal{T}_h\}$, with

$$F_\Gamma^a := |\Gamma|^{-1} \int_\Gamma v d\gamma \quad \text{or} \quad F_\Gamma^b := v(m_\Gamma) \quad (m_\Gamma \text{ midpoint of edge } \Gamma) \tag{13}$$

such that the finite element spaces can be written as

$$\begin{aligned} W_h^{a,b} := \{&v \in L^2(\Omega_h), v \in \tilde{Q}_1(T), \forall T \in \mathcal{T}_h, v \text{ continuous w.r.t. all} \\ &\text{nodal functionals } F_{\Gamma_{i,j}}^{a,b}(\cdot), \text{ and } F_{\Gamma_{i0}}^{a,b}(v) = 0, \forall \Gamma_{i0}\}. \end{aligned} \tag{14}$$

Here, $\Gamma_{i,j}$ means all inner edges sharing the two elements i and j, while Γ_{i0} denotes the boundary edges of $\partial\Omega_h$. In this paper, we always employ version 'a' with the integral mean values as degrees of freedom. Then, the corresponding discrete functions will be approximated in the spaces

$$V_h := W_h^a \times W_h^a \,,\; L_h := \left\{q_h \in L_0^2(\Omega), q_{h|T} = \text{const.} \,, \forall \mathcal{T} \in \mathcal{T}_h\right\}. \tag{15}$$

Due to the nonconformity of the discrete velocities, the classical discrete Korn's inequality is not satisfied which is important for problems involving the symmetric part of the gradient. Therefore, appropriate edge-oriented stabilization techniques (see [3], [4], [7]) have to be included which directly treat the jump across the inter-elementary boundaries via adding the following bilinear form

$$\sum_{edges E} \frac{1}{|E|} \int_E [\phi_i][\phi_j] d\sigma \tag{16}$$

for all basis functions ϕ_i and ϕ_j of $W_h^{a,b}$. Taking into account an additional relaxation parameter $s = s(\nu)$, the corresponding stiffness matrices are defined via the edge-oriented stabilization term:

$$\langle \mathbf{S}\boldsymbol{u}, \boldsymbol{v}\rangle = s \sum_{E \in E_I \cup E_D} \frac{1}{|E|} \int_E [\boldsymbol{u}][\boldsymbol{v}] d\sigma \tag{17}$$

Here, the jump of a function $\boldsymbol{u}$ on an edge E is given by

$$[\boldsymbol{u}] = \begin{cases} \boldsymbol{u}^+ \cdot \boldsymbol{n}^+ + \boldsymbol{u}^- \cdot \boldsymbol{n}^- & \text{on internal edges } E_I \,, \\ \boldsymbol{u} \cdot \boldsymbol{n} & \text{on Dirichlet boundary edges } E_D, \\ 0 & \text{on Neumann boundary edges } E_N, \end{cases} \tag{18}$$

where $\boldsymbol{n}$ is the outward normal to the edge and $(\cdot)^+$ and $(\cdot)^-$ indicate the value of the generic quantity $(\cdot)$ on the two elements sharing the same edge. For a detailed description of the analysis for this stabilization technique, we refer to [3] and [4], while a description of related numerical and algorithmic approaches can be found in [7].

In contrast to the described conforming Stokes Element Q_2/P_1, the approximation error for the velocity in the L^2-norm is of order $O(h^2)$ for the 'linear' nonconforming element pair $\tilde{Q}_1/Q_0$. However, the realization and analysis of appropriate stabilization techniques for the case of higher Reynolds numbers is possible and is reported in several papers (see for instance [6] and [14]). Moreover, these special upwinding and streamline-diffusion techniques have been realized in the FEATFLOW software which has been successfully applied to a wide range of realistic flow configurations (see [16]). On the other hand, such stabilization techniques are - in contrast to a pure Galerkin discretization resp. to central differencing for the convective terms - very closely related to special additional parameters which have to be chosen by the user in a more or less clever way: We will shortly discuss the influence of such 'free' parameters onto the global approximation behavior and hence the total efficiency.

4 Nonlinear Solvers

4.1 Discrete Newton solver

After applying the discretization method to the system (1) where the approximations belong to the finite dimensional spaces (8) and (9), we obtain a system of nonlinear algebraic equations which can be represented as

$$\mathcal{R}(\boldsymbol{x}) = \mathbf{0}, \tag{19}$$

where $\boldsymbol{x}$ represents the vector of the coefficients corresponding to the unknowns $(\boldsymbol{v}_h, p_h)$. To solve this system we apply a Newton iteration with damping which results in iterations of the form

$$\boldsymbol{x}^{n+1} = \boldsymbol{x}^n + \omega^n \left[\frac{\partial \mathcal{R}(\boldsymbol{x}^n)}{\partial \boldsymbol{x}}\right]^{-1} \mathcal{R}(\boldsymbol{x}^n). \tag{20}$$

This iteration is repeated until a prescribed convergence criterion is satisfied, i.e., a certain norm of the residual term $\|\mathcal{R}(\boldsymbol{x}^n)\|$ is small enough. The damping parameter $\omega^n \in [-1, 0)$ is chosen such that

$$\mathcal{R}(\boldsymbol{x}^{n+1}) \cdot \boldsymbol{x}^{n+1} \leq \mathcal{R}(\boldsymbol{x}^n) \cdot \boldsymbol{x}^n. \tag{21}$$

This damping significantly improves the robustness of the Newton iteration in the case when the current approximation $\boldsymbol{x}^n$ is not close enough to the final solution and the Newton method without damping is not guaranteed to converge.

The Jacobian matrix $\left[\frac{\partial \mathcal{R}(\boldsymbol{x}^n)}{\partial \boldsymbol{x}}\right]$ is not computed exactly in our code, instead its approximation is computed using divided differences as

$$\left[\frac{\partial \mathcal{R}(\boldsymbol{x}^n)}{\partial \boldsymbol{x}}\right]_{ij} \approx \frac{\mathcal{R}_i(\boldsymbol{x}^n + \varepsilon \boldsymbol{e}_j) - \mathcal{R}_i(\boldsymbol{x}^n - \varepsilon \boldsymbol{e}_j)}{2\varepsilon}, \tag{22}$$

where $\boldsymbol{e}_j$ is the vector with unit j-th component and zero otherwise. The parameter ε can be fixed or can be modified according to some norm of the solution $\|\boldsymbol{x}^n\|$ or the norm of the update in the previous step, i.e., $\|\boldsymbol{x}^n - \boldsymbol{x}^{n-1}\|$. In the subsequent numerical tests, we will compare this discrete approach with the following continuous method, not only w.r.t. the nonlinear convergence behavior, but also checking the sensitivity of the overall nonlinear behavior in relation to this 'free' parameter ε.

4.2 Continuous Newton solver

Diffusive term In this approach, the nonlinearity is handled on the continuous variational level. Let $\boldsymbol{u}^l$ being the initial state, the (continuous) Newton method consists of finding $\boldsymbol{u} \in V$ such that

$$\begin{aligned}\int_\Omega & 2\nu(D_{\mathrm{II}}(\boldsymbol{u}^l))\mathbf{D}(\boldsymbol{u}) : \mathbf{D}(\boldsymbol{v})dx \\ & + \int_\Omega 2\nu'(D_{\mathrm{II}}(\boldsymbol{u}^l))[\mathbf{D}(\boldsymbol{u}^l) : \mathbf{D}(\boldsymbol{u})][\mathbf{D}(\boldsymbol{u}^l) : \mathbf{D}(\boldsymbol{v})]dx \\ & = \int_\Omega \boldsymbol{f}\boldsymbol{v}dx - \int_\Omega 2\nu(D_{\mathrm{II}}(\boldsymbol{u}^l))\mathbf{D}(\boldsymbol{u}^l) : \mathbf{D}(\boldsymbol{v})dx, \quad \forall \boldsymbol{v} \in V\,, \end{aligned} \tag{23}$$

where $\nu'(\cdot)$ is the derivative of $\nu(\cdot)$. To see this, set $\boldsymbol{y} = \mathbf{D}(\boldsymbol{u}^l), \boldsymbol{z} = \mathbf{D}(\boldsymbol{u}), F(\boldsymbol{y}) = \nu(\frac{1}{2}|\boldsymbol{y}|^2)\boldsymbol{y}$ and $f(t) = F(\boldsymbol{y} + t\boldsymbol{z})$, so that

$$\partial_j F_i(\boldsymbol{y}) = \nu'(\frac{1}{2}|\boldsymbol{y}|^2)y_j y_i + \nu(\frac{1}{2}|\boldsymbol{y}|^2)\delta_{ij}\,, \tag{24}$$

where δ_{ij} stands for the standard Kronecker symbol. Having

$$\begin{aligned} f_i'(t) &= \textstyle\sum_j \partial_j F_i(\boldsymbol{y} + t\boldsymbol{z})z_j \\ &= \nu'(\tfrac{1}{2}|\boldsymbol{y} + t\boldsymbol{z}|^2)\langle \boldsymbol{y}, \boldsymbol{z}\rangle y_i + \nu(\tfrac{1}{2}|\boldsymbol{y} + t\boldsymbol{z}|^2)z_i\,, \end{aligned} \tag{25}$$

we decrease t towards zero, such that we obtain the Frechet derivative:

$$\nabla \cdot [2\nu(D_{II}(\boldsymbol{u}^l))\mathbf{D}(\boldsymbol{u}) + 2\nu^{'}(D_{II}(\boldsymbol{u}^l))(\mathbf{D}(\boldsymbol{u}^l) : \mathbf{D}(\boldsymbol{u}))\mathbf{D}(\boldsymbol{u}^l)] \tag{26}$$

Finally, the weak formulation of (26) leads to the relation given in (23). Therefore, the algorithm consists of finding $(\boldsymbol{u}, p)$ as solution of the nonlinear discrete system

$$\begin{cases} \mathbf{A}(\boldsymbol{u}^l)\boldsymbol{u} + \delta_d \mathbf{A}^*(\boldsymbol{u}^l)\boldsymbol{u} + \mathbf{B}p = R_u(\boldsymbol{u}^l, p^l), \\ \mathbf{B}^T\boldsymbol{u} \qquad\qquad\qquad\qquad\quad = R_p(\boldsymbol{u}^l, p^l), \end{cases} \tag{27}$$

where $R_u(\cdot,\cdot)$ and $R_p(\cdot,\cdot)$ denote the corresponding nonlinear residual terms for the momentum and continuity equations, and the matrix $\mathbf{A}^*(\boldsymbol{u}^l)$ is related to the bilinear form

$$\langle \mathbf{A}^*(\boldsymbol{u}^l)\boldsymbol{u}, \boldsymbol{v}\rangle = \int_\Omega 2\nu^{'}(D_{II}(\boldsymbol{u}^l))[\mathbf{D}(\boldsymbol{u}^l) : \mathbf{D}(\boldsymbol{u})][\mathbf{D}(\boldsymbol{u}^l) : \mathbf{D}(\boldsymbol{v})]dx. \tag{28}$$

Convective term The corresponding Newton linearization applied to the convective term $\langle \mathbf{N}(\boldsymbol{u})\boldsymbol{u}, \boldsymbol{v}\rangle$ leads to the additional bilinear form

$$\langle \mathbf{N}(\boldsymbol{u}^l)\boldsymbol{u}, \boldsymbol{v}\rangle + \delta_c \langle \mathbf{N}^*(\boldsymbol{u}^l)\boldsymbol{u}, \boldsymbol{v}\rangle, \; \forall \boldsymbol{v} \in X\,, \tag{29}$$

with $\langle \mathbf{N}^*(\boldsymbol{u}^l)\boldsymbol{u}, \boldsymbol{v}\rangle = \int_\Omega (\boldsymbol{u} \cdot \nabla \boldsymbol{u}^l)\boldsymbol{v}dx$ for all $\boldsymbol{v} \in X$. Then, the complete algorithm consists of finding $(\boldsymbol{u}, p)$ as solution of the following linear matrix-vector system

$$\begin{cases} \mathbf{A}(\boldsymbol{u}^l)\boldsymbol{u} + \delta_d \mathbf{A}^*(\boldsymbol{u}^l)\boldsymbol{u} + \mathbf{N}(\boldsymbol{u}^l)\boldsymbol{u} + \delta_c \mathbf{N}^*(\boldsymbol{u}^l)\boldsymbol{u} + \mathbf{B}p = R_u(\boldsymbol{u}^l, p^l), \\ \mathbf{B}^T\boldsymbol{u} \qquad\qquad\qquad\qquad\qquad\qquad\qquad\qquad\quad = R_p(\boldsymbol{u}^l, p^l). \end{cases} \tag{30}$$

Once the auxiliary solution $(\boldsymbol{u}, p)$ is determined, the current approximation is updated, with ω^l as appropriate relaxation parameter:

$$(\boldsymbol{u}^{l+1}, p^{l+1}) = (\boldsymbol{u}^l, p^l) + \omega^l(\boldsymbol{u}, p) \tag{31}$$

The full Newton method is supplied for $\delta_d = 1$ and $\delta_c = 1$, while the fixpoint method corresponds to $\delta_d = 0$ and $\delta_c = 0$.

It is well-known that the 'standard' discretization of the convective part, i.e. with central discretization, may lead to numerical problems, namely to:

- stiffness matrices not of positive type ('M-matrix properties'), so the iterative schemes such as multigrid will not lead to efficient convergence results.
- oscillations and deteriorations of the discrete solutions which have purely numerical character.

To stabilize the convective term in the FEM context, there are two approaches which are widely used in the CFD community: *upwind* schemes and *streamline-diffusion* techniques. However, these two stabilization techniques may veil the (potentially) quadratic convergence of the Newton methods, unless if we compute the Jacobian matrix for the stabilization terms, too. For streamline-diffusion, the additional stabilization of the Newton linearization may be supplied in the same manner as it was done previously for the nonlinear viscosity, while upwind stabilization techniques require special treatment of $\langle \mathbf{N}^*(\boldsymbol{u}^l)\boldsymbol{u}, \boldsymbol{v}\rangle$. We will show the resulting nonlinear and linear convergence behavior with Newton and fixpoint methods for both upwind and streamline-diffusion stabilization techniques.

5 Linear Solvers

This section is devoted to give a brief description of the involved solution techniques for the resulting linear systems. For the nonconforming Stokes element $\tilde{Q}_1/Q_0$, a 'local pressure Schur complement' preconditioner (see [13] and [14]) as generalization of so-called 'Vanka smoothers' (see [18]) is constructed on patches Ω_i which are ensembles of one or several mesh cells, and this local preconditioner is embedded as global smoother into an outer block Jacobi/Gauss-Seidel iteration which acts directly on the coupled systems of Stokes, resp. of Oseen type. If we denote by $\tilde{R}_u$ and $\tilde{R}_p$ the discrete residuals for the complete momentum and continuity equation which include the complete stabilization term due to the bilinear form $\mathbf{S}$ as defined in (17), one smoothing step in defect-correction notation can be described as

$$\begin{bmatrix} \boldsymbol{u}^l \\ p^l \end{bmatrix} = \begin{bmatrix} \boldsymbol{u}^{l-1} \\ p^{l-1} \end{bmatrix} + \omega^l \sum_i \begin{pmatrix} \mathbf{F} + \mathbf{S}^*_{|\Omega_i} & \tilde{\mathbf{B}}_{|\Omega_i} \\ \tilde{\mathbf{B}}^T_{|\Omega_i} & 0 \end{pmatrix}^{-1} \begin{bmatrix} \tilde{R}_u(\boldsymbol{u}^{l-1}, p^{l-1}) \\ \tilde{R}_p(\boldsymbol{u}^{l-1}, p^{l-1}) \end{bmatrix} \tag{32}$$

with matrix $\mathbf{F} = \tilde{\mathbf{A}} + \delta_d \tilde{\mathbf{A}}^* + \tilde{\mathbf{N}} + \delta_c \tilde{\mathbf{N}}^*$. For the preconditioning step, only a part of the full matrix, i.e. $\mathbf{F} + \mathbf{S}^*$ instead of $\mathbf{F} + \mathbf{S}$, is involved (see [7] for the details). All other components in the multigrid approach, that means intergrid transfer, coarse grid correction and coarse grid solver, are quite standard and are based on the underlying hierarchical mesh hierarchy and the properties of the nonconforming finite elements [14].

For the biquadratic conforming Stokes Element Q_2/P_1, a standard GMRES method [10] as typical iterative single grid solver with ILU preconditioning is applied. The preconditioner is taken from the library developed in [2]. It is clear that multigrid might be preferable, too, but up to now, corresponding Vanka-like smoothers for this Q_2/P_1 ansatz are not yet available; in fact, they are the target of intensive research studies in our projects. Anyway, this GMRES solver is probably the most common approach in the CFD community, besides using BiCGSTAB [17], such that it is quite important to perform these comparisons with the multigrid solver.

6 Numerical Comparisons

In this section, we present the results from our numerical experiments with various parameters settings and also different physical models for the both proposed discretization and solution frameworks. The computational domain is always a channel geometry with an interior circle as shown via the coarsest mesh in the following figure; this configuration is following the standard CFD benchmark 'Flow around cylinder' [12]. The reader should know the the position of the circle is slightly non-symmetric w.r.t. the height such that the lift coefficient is non-homogeneous.

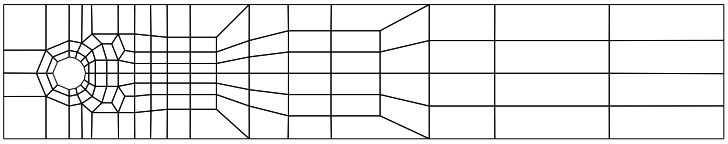

Mesh information			$\tilde{Q}_1/Q_0$	Q_2/P_1
Level	Elements	Vertices	Total unknowns	Total unknowns
1	156	130	702	1533
2	572	520	2686	5927
3	2184	2080	10608	23295
4	8528	8320	42016	92351
5	33696	33280	167232	367743
6	133952	133120	667264	–

Table 1. Coarse mesh and geometrical details for the 'Flow around cylinder' configuration for the both Stokes elements $\tilde{Q}_1/Q_0$ and Q_2/P_1 on the different levels of mesh refinement.

6.1 Constant viscosity test case

The first computational tests are performed for the Newtonian Navier-Stokes equations, i.e. with constant viscosity, so the only source of nonlinearity is the convective term. To be in the limit of steady flows, the Reynolds number - by variations of the viscosity parameter only - is kept to be less than $Re = 50$ which is near the critical point to turn into (periodically) oscillating flow behavior. Although the cases $Re = 20$ (the standard test in [12]) and also $Re = 50$ appear to be far away from transport-dominated flows, nevertheless the involved convective term requires special treatment: While the simulations show that the approximation results for such 'medium' Reynolds numbers seem to be the best for no stabilization at all, that means applying central differencing or the pure Galerkin formulation, the involved multigrid routines are much more sensitive. Therefore, in the case of the rotated bilinear nonconforming Stokes element $\tilde{Q}_1/Q_0$, we apply the two standard techniques

of streamline-diffusion (SD) and upwind (UPW) stabilization (see [14] for details of the discretization). However, such methods require additional 'free' parameters as the local mesh width, the relation to the local Re number and an additional relaxation parameter, which all of them lead to the non-trivial task of parameter tuning, particularly in the case of nonlinear flow models and/or on non-uniform meshes. In contrast, the conforming Q_2/P_1 element is employed - as usually - without any stabilization which seems to be sufficient in our case of low up to medium Re numbers. However, we also have to state that, up to now, it is by far not clear of how to develop corresponding stabilization techniques which can be adapted to the potentially available higher order accuracy of this Stokes element in the case of much larger Re numbers.

The following tables show the resulting approximation properties w.r.t. the measured drag and lift coefficient on the different refinement levels, the required nonlinear iteration numbers #NN to gain 8 digits (here we compare the continuous resp. discrete Newton solver with the simpler fixpoint approach) and the corresponding averaged number #NL of linear iterations per nonlinear cycle to gain 2 digits. We apply the described multigrid solver for the $\tilde{Q}_1/Q_0$ element, while for the conforming Q_2/P_1 element, the preconditoned GMRES solver has been used. These approximation and solution properties are shown with the corresponding CPU times.

The results from these tables are quite prototypical for similar configurations with low up to medium Re numbers and can be concluded as follows:

1. Both discretizations lead to the same results if we apply sufficiently many grid refinement steps; as expected, the quadratic Q_2/P_1 approach is more accurate which can be summarized by the following thumb rules:
   'The linear $\tilde{Q}_1/Q_0$ approach requires - depending on the specific choice of the stabilization technique for the convective term - about 1 or 2 further levels of grid refinement to produce a comparable accuracy as the quadratic Q_2/P_1 ansatz. That means, the required number of elements is about 5 - 20 times larger which can result in approximately up to 10 times more unknowns (see Table 1). However, keep in mind that the corresponding differences regarding the amount of RAM storage are much smaller since the matrix stencil for the higher-order FEM is significantly bigger!'
2. We clearly see the typical effect of 'optimal' multigrid: the linear convergence rates are in the range of $\rho_{MG} \approx 0.1$ (only 2 - 4 steps to gain two digits are required) and quite independent of the mesh size and also the underlying Re numbers. It is remarkable that the solution of the non-symmetric Oseen equations is often 'easier' than solving symmetric Stokes problems!
   In contrast, the GMRES solver shows the expected mesh-dependent convergence behavior which is quantitatively much worse than the corresponding multigrid approach. Refining the mesh does not only lead to

$\tilde{Q}_1/Q_0$ - SD			
Level	Stokes	$Re = 20$	$Re = 50$
3	3.0560×10^3	5.7365×10^0	3.9976×10^0
4	3.1191×10^3	5.6679×10^0	3.8516×10^0
5	3.1364×10^3	5.6161×10^0	3.7572×10^0
6	3.1409×10^3	5.5925×10^0	3.7167×10^0
$\tilde{Q}_1/Q_0$ - UPW			
Level	Stokes	$Re = 20$	$Re = 50$
3	3.0560×10^3	5.5833×10^0	3.9580×10^0
4	3.1191×10^3	5.5737×10^0	3.7662×10^0
5	3.1364×10^3	5.5769×10^0	3.7085×10^0
6	3.1409×10^3	5.5788×10^0	3.6972×10^0
Q_2/P_1 - central			
Level	Stokes	$Re = 20$	$Re = 50$
2	3.1237×10^3	5.5569×10^0	3.6677×10^0
3	3.1374×10^3	5.5728×10^0	3.6867×10^0
4	3.1411×10^3	5.5777×10^0	3.6925×10^0
5	3.1421×10^3	5.5791×10^0	3.6940×10^0

$\tilde{Q}_1/Q_0$ - SD			
Level	Stokes	$Re = 20$	$Re = 50$
3	2.8240×10^1	0.6431×10^{-2}	-1.0423×10^{-2}
4	3.0158×10^1	0.8341×10^{-2}	-1.1131×10^{-2}
5	3.0684×10^1	0.9691×10^{-2}	-1.0977×10^{-2}
6	3.0820×10^1	1.0281×10^{-2}	-1.0850×10^{-2}
$\tilde{Q}_1/Q_0$ - UPW			
Level	Stokes	$Re = 20$	$Re = 50$
3	2.8238×10^1	0.4754×10^{-2}	-1.3578×10^{-2}
4	3.0157×10^1	0.9536×10^{-2}	-9.9338×10^{-3}
5	3.0684×10^1	1.0455×10^{-2}	-1.0010×10^{-2}
6	3.0820×10^1	1.0593×10^{-2}	-1.0479×10^{-2}
Q_2/P_1 - central			
Level	Stokes	$Re = 20$	$Re = 50$
2	2.9854×10^1	0.9512×10^{-2}	-1.1764×10^{-2}
3	3.0578×10^1	1.0609×10^{-2}	-1.0894×10^{-2}
4	3.0788×10^1	1.0616×10^{-2}	-1.0739×10^{-2}
5	3.0846×10^1	1.0617×10^{-2}	-1.0730×10^{-2}

Table 2. Drag coefficient (top) and lift coefficient (bottom) for different Re numbers and for various levels of mesh refinement for the $\tilde{Q}_1/Q_0$ (with streamline-diffusion and upwinding for the stabilization of the convective term) and the Q_2/P_1 approach (with no stabilization at all).

bigger problem sizes, but also to significantly more linear iteration sweeps due to the increasing condition number of the discrete matrices.

$\tilde{Q}_1/Q_0$ - SD							
		Stokes		$Re = 20$		$Re = 50$	
Level	Nonlinear scheme	#NN/#NL	CPU	#NN/#NL	CPU	#NN/#NL	CPU
3	Fixpoint	4/2	9	11/3	19	17/4	41
	Newton	4/3	9	8/3	18	9/3	19
4	Fixpoint	4/3	26	10/3	59	16/3	110
	Newton	4/3	27	6/3	41	7/3	53
5	Fixpoint	4/3	113	9/3	206	14/3	346
	Newton	4/3	109	5/2	114	6/3	137
6	Fixpoint	4/4	551	8/3	671	12/2	989
	Newton	4/4	522	5/3	562	6/3	601

$\tilde{Q}_1/Q_0$ - UPW							
		Stokes		$Re = 20$		$Re = 50$	
Level	Nonlinear scheme	#NN/#NL	CPU	#NN/#NL	CPU	#NN/#NL	CPU
3	Fixpoint	4/3	9	10/4	35	16/4	53
	Newton	4/3	9	8/4	26	11/5	46
4	Fixpoint	4/3	25	10/3	78	15/3	143
	Newton	4/3	25	6/3	47	7/3	71
5	Fixpoint	4/3	106	10/3	246	14/3	386
	Newton	4/3	107	5/3	116	6/3	174
6	Fixpoint	4/4	505	8/2	633	12/3	1194
	Newton	4/4	516	5/3	525	6/3	535

Q_2/P_1 - central							
		Stokes		$Re = 20$		$Re = 50$	
Level	Nonlinear scheme	#NN/#NL	CPU	#NN/#NL	CPU	#NN/#NL	CPU
2	Fixpoint	4/24	8	12/35	26	18/38	40
	Newton	4/24	7	6/32	11	7/44	14
3	Fixpoint	4/52	49	12/67	172	17/78	271
	Newton	4/51	42	6/69	76	7/81	102
4	Fixpoint	4/134	400	11/116	1029	16/149	1878
	Newton	4/135	393	6/122	534	7/163	885
5	Fixpoint	5/586	9726	11/348	12457	16/315	16193
	Newton	4/541	7184	6/302	6326	6/330	6250

Table 3. Corresponding results for the total number of nonlinear iterations (#NN) and the averaged number of linear sweeps (#NL) per nonlinear cycle together with the elapsed CPU time.

3. The advantage of the more complex Newton solvers in comparison to the 'simple' fixpoint approach is not so obvious: Even in the $Re = 50$ case, the required number of nonlinear fixpoint steps is only 2 - 3 times larger than compared with the Newton variants. However, in contrast to the linear solvers, the nonlinear convergence behavior is only related to the properties of the underlying continuous (!) problem, that means the Re

number in our case. This is in contrast to the linear problems which are mainly depending on the condition numbers of the matrices and hence on the mesh width resp. the mesh topology.

Scheme-Level	Drag	Lift	#NN/#NL	CPU
Q_2/P_1 - central - LEV2	0.9512×10^{-2}	5.5569×10^{0}	6/32	11
Q_2/P_1 - central - LEV3	1.0609×10^{-2}	5.5728×10^{0}	6/69	76
Q_2/P_1 - central - LEV4	1.0616×10^{-2}	5.5777×10^{0}	6/122	534
Q_2/P_1 - central - LEV5	1.0617×10^{-2}	5.5791×10^{0}	6/302	6326
$\tilde{Q}_1/Q_0$ - UPW - LEV3	0.4754×10^{-2}	5.5833×10^{0}	8/4	26
$\tilde{Q}_1/Q_0$ - UPW - LEV4	0.9536×10^{-2}	5.5737×10^{0}	6/3	47
$\tilde{Q}_1/Q_0$ - UPW - LEV5	1.0455×10^{-2}	5.5769×10^{0}	5/3	116
$\tilde{Q}_1/Q_0$ - UPW - LEV6	1.0593×10^{-2}	5.5788×10^{0}	5/3	525

Table 4. Direct comparison of the Q_2/P_1 approach vs. the $\tilde{Q}_1/Q_0$ Stokes element (with upwinding) for $Re = 20$ (standard stationary CFD benchmark configuration in [12]).

As a first summary, we can state that - as expected - the quadratic Q_2/P_1 is more accurate for the considered low up to medium Re numbers which lead to steady state solutions. That means, the 'simpler' $\tilde{Q}_1/Q_0$ approach may require approximately 5 - 20 times more grid points. On the other hand, the corresponding direct multigrid solver for the $\tilde{Q}_1/Q_0$ element pair shows the typical 'optimal' convergence behavior which is in contrast to the preconditioned GMRES solver: The single-grid approach shows convergence rates which clearly depend on the mesh width and which are quantitatively much worse.

Therefore, concerning the total efficiency, the '$\tilde{Q}_1/Q_0$ + multigrid' combination is (still) preferable. It is obvious that a higher order discretization has a high potential for the future, but the comparisons demonstrate that discretization and solver aspects have to be treated as a unit! Hence, the analogous development of robust and efficient multigrid techniques for the Q_2/P_1 and similar high-order Stokes elements is a must for future research and will have high priority in our own research activities.

6.2 Non-constant viscosity test case

Since the examined nonlinearity related to the convective term in the case of a steady state solution is quite moderate, our next tests are concerned with the discussed nonlinear viscosity functions. As a first consequence, the equivalence between the gradient and the deformation tensor formulations for the diffusive part are not valid any more, so the stabilized version of the rotated bilinear element pair $\tilde{Q}_1/Q_0$ is required.

The following tables show the results for the regularized *power paw* model, that means $\nu(\boldsymbol{u}) = (\varepsilon + D_{II}(\boldsymbol{u}))^{-\alpha/2}$, $\varepsilon = 10^{-2}$, which has been integrated

into both described Navier-Stokes solvers; the geometrical configuration corresponds to the previous 'Flow around cylinder' configuration, too. Again, we calculate the lift and drag coefficients, and additionally the mean pressure difference $\triangle\, p$ on the cylinder (see [12]). Due to the fact that the considered flow is very slow, the computation was done without the convective term such that - for numerical test reasons - the nonlinear viscosity is the only source of nonlinearity. However, the calculations show that the strength of the nonlinear behavior for the chosen parameters $\alpha = 0.5$ and particularly $\alpha = 0.9$ is quite significant.

The results for these non-Newtonian test cases are quite similar as those for the Newtonian flow model: Again, the quadratic Q_2/P_1 approach is more accurate while the corresponding GMRES solver for the linear subproblems in each Newton step shows the well-known grid dependent convergence behavior. In contrast, the performed multigrid solver in the $\tilde{Q}_1/Q_0$ context is robust against variations in the mesh width and also w.r.t. the problem-specific parameter α which mainly determines the corresponding nonlinear behavior.

$\nu(\boldsymbol{u}) = (\varepsilon + D_{\mathrm{II}}(u))^{-\alpha/2}$					
Level	Stokes element	Drag	Lift	$\triangle\, p$	#NN/#NL
$\alpha = 0.5$					
2	$\tilde{Q}_1/Q_0$	1409.60	11.86	22.41	6/2
	Q_2/P_1	1607.10	14.48	25.38	6/27
3	$\tilde{Q}_1/Q_0$	1554.10	13.70	23.99	8/2
	Q_2/P_1	1629.10	14.27	25.16	8/65
4	$\tilde{Q}_1/Q_0$	1594.20	14.25	24.56	9/2
	Q_2/P_1	1635.80	14.39	25.09	8/140
5	$\tilde{Q}_1/Q_0$	1615.60	14.43	24.81	8/2
	Q_2/P_1	1637.60	14.44	25.07	9/723
6	$\tilde{Q}_1/Q_0$	1626.20	14.46	24.94	8/2
$\alpha = 0.9$					
2	$\tilde{Q}_1/Q_0$	819.49	2.5201	14.22	13/2
	Q_2/P_1	920.59	2.1805	16.76	17/37
3	$\tilde{Q}_1/Q_0$	917.89	3.1958	15.54	14/2
	Q_2/P_1	941.51	3.3310	16.02	14/93
4	$\tilde{Q}_1/Q_0$	916.02	3.7381	15.74	12/2
	Q_2/P_1	953.94	3.9217	15.82	19/294
5	$\tilde{Q}_1/Q_0$	935.13	3.9954	15.82	15/3
	Q_2/P_1	957.64	4.0587	15.87	18/1162
6	$\tilde{Q}_1/Q_0$	946.22	4.0592	15.85	13/5

Table 5. Comparison of approximation results (drag, lift pressure difference) and of the total number of nonlinear iterations (#NN) and the averaged number of linear sweeps (#NL) per Newton step.

6.3 Examination of the Newton variants

In the final simulations, we examine the characteristics of the chosen nonlinear solvers of Newton type. To be precise, in the case of the continuous Newton approach we demonstrate the importance of including all terms of the Jacobi matrix in contrast to the simpler fixpoint approach which utilizes the partial differential operator only, hereby evaluated for the results of the last nonlinear iteration step (see in (30)).

	$\alpha = 0.5$				$\alpha = 0.9$			
	Newton		Fixpoint		Newton		Fixpoint	
Level	#NN/#NL	CPU	#NN/#NL	CPU	#NN/#NL	CPU	#NN/#NL	CPU
2	6/2	11	19/2	37	13/2	60	74/2	228
3	8/2	46	18/2	126	14/2	215	114/2	1359
4	9/2	199	16/2	389	12/2	740	125/2	5871
5	8/2	707	14/2	1517	15/3	3957	119/2	21735
6	8/2	2885	12/2	5047	13/5	25926	109/2	80438

Table 6. Direct comparison of continuous Newton vs. fixpoint method for the treatment of the nonlinearity with the $\tilde{Q}_1/Q_0$ Stokes element.

The results in Table 6 show the corresponding comparison for the nonconforming $\tilde{Q}_1/Q_0$ element. In both cases, for the full Newton and the simplified fixpoint approach, the described multigrid solvers for the linear auxiliary problems have been applied to gain 2 digits of relative accuracy. While for the moderate case of $\alpha = 0.5$, the differences are not so significant, the harder test case $\alpha = 0.9$ shows the importance of a fully developed Newton solver: Differences of order 4 - 8 w.r.t. the number of nonlinear iterations occur while the averaged number of linear sweeps remains (more or less) constant such that big differences in the total efficiency are typical for such flow problems.

Finally, we discuss the sensitivity of the discrete Newton approach via divided differences regarding the involved step-length parameter ε, the mesh width h and the problem-dependent parameter α which is responsible for the strength of the nonlinearity. As explained in (22), the discrete Jacobi matrix is calculated via:

$$\left[\frac{\partial \mathcal{R}(\boldsymbol{x}^n)}{\partial \boldsymbol{x}}\right]_{ij} \approx \frac{\mathcal{R}_i(\boldsymbol{x}^n + \varepsilon \boldsymbol{e}_j) - \mathcal{R}_i(\boldsymbol{x}^n - \varepsilon \boldsymbol{e}_j)}{2\varepsilon} \tag{33}$$

Therefore, in the following tables we examine more carefully the resulting discrete Jacobi matrices w.r.t. the discussed parameters ε, h and α, and we show how the 'outer' nonlinear convergence behavior as well as the 'inner' linear solution behavior is influenced by the resulting matrix .

$\varepsilon \setminus$ TOL	10^{-1}	10^{-2}	10^{-3}	10^{-4}
10^{-2}	40*/ 4 [60]	32/ 7 [49]	30/ 13 [48]	21/ 20 [36]
10^{-3}	14/ 12 [22]	10/ 16 [16]	8/ 24 [14]	8/ 29 [15]
10^{-4}	10/ 15 [16]	8/ 19 [13]	6/ 27 [11]	7/ 29 [13]
10^{-5}	10/ 15 [16]	8/ 19 [13]	6/ 27 [11]	7/ 29 [13]
10^{-6}	10/ 15 [16]	8/ 19 [13]	6/ 27 [11]	7/ 29 [13]
10^{-7}	10/ 15 [16]	8/ 19 [13]	6/ 27 [11]	7/ 29 [13]
10^{-8}	10/ 15 [16]	8/ 19 [13]	6/ 27 [11]	7/ 29 [13]

$\varepsilon \setminus$ TOL	10^{-1}	10^{-2}	10^{-3}	10^{-4}
10^{-2}	40*/ 7 [280]	40*/ 14 [305]	40*/ 22 [335]	37/ 36 [358]
10^{-3}	33/ 24 [288]	14/ 35 [134]	10/ 57 [120]	11/ 67 [145]
10^{-4}	11/ 40 [113]	10/ 40 [103]	8/ 65 [105]	8/ 70 [114]
10^{-5}	11/ 38 [113]	9/ 43 [99]	8/ 65 [109]	8/ 70 [110]
10^{-6}	11/ 38 [114]	9/ 43 [97]	8/ 65 [105]	8/ 70 [111]
10^{-7}	21/ 25 [189]	21/ 35 [212]	13/ 58 [167]	14/ 78 [207]
10^{-8}	21/ 23 [185]	15/ 40 [160]	11/ 62 [146]	15/ 82 [234]

$\varepsilon \setminus$ TOL	10^{-1}	10^{-2}	10^{-3}	10^{-4}
10^{-2}	40*/ 11 [1306]	40*/ 23 [1548]	40*/ 51 [2055]	40*/ 84 [2720]
10^{-3}	40*/ 33 [1745]	31/ 48 [1561]	16/ 102 [1314]	18/ 129 [1877]
10^{-4}	15/ 85 [1124]	11/ 104 [983]	9/ 134 [999]	9/ 199 [1399]
10^{-5}	11/ 101 [976]	9/ 100 [807]	8/ 140 [941]	9/ 204 [1423]
10^{-6}	11/ 100 [954]	9/ 100 [798]	8/ 139 [920]	9/ 204 [1426]
10^{-7}	10/ 104 [898]	15/ 97 [1320]	10/ 138 [1148]	13/ 219 [2241]
10^{-8}	40*/ 29 [1814]	40*/ 156 [5174]	40*/ 199 [6244]	40*/ 274 [8108]

$\varepsilon \setminus$ TOL	10^{-1}	10^{-2}	10^{-3}	10^{-4}
10^{-2}	diverg.	40*/ 57 [10153]	40*/ 122 [17075]	40*/ 245 [31638]
10^{-3}	40*/ 35 [8251]	40*/ 82 [13550]	26/ 214 [18679]	22/ 348 [25640]
10^{-4}	20/ 181 [13244]	16/ 264 [14637]	14/ 432 [20002]	9/ 755 [22325]
10^{-5}	11/ 296 [11331]	8/ 492 [12978]	9/ 723 [22105]	8/ 944 [25220]
10^{-6}	25/ 148 [13947]	10/ 374 [12388]	14/ 383 [18271]	11/ 590 [22030]
10^{-7}	40*/ 255 [37031]	27/ 479 [44067]	20/ 757 [50167]	19/ 811 [50788]
10^{-8}	40*/ 252 [36063]	40*/ 245 [28289]	40*/356 [47587]	40*/ 472 [62539]

Table 7. Direct comparison of the results for the discrete Newton approach with the Q_2/P_1 Stokes element for $\alpha = 0.5$; the parameters ε and TOL as step-length parameter, resp., as stopping criterion are varied. The results are shown for grid refinement level 2 (top) up to level 5 (bottom). We always provide the total number of nonlinear iterations (#NN), the averaged number of linear sweeps (#NL) per Newton step and the elapsed CPU time in seconds (in brackets). The maximum number of nonlinear Newton steps is 40.

$\varepsilon \setminus$ TOL	10^{-1}	10^{-2}	10^{-3}	10^{-4}
10^{-2}	40⋆/ 6 [62]	40⋆/ 15 [67]	40⋆/ 27 [74]	40⋆/ 34 [79]
10^{-3}	26/ 15 [43]	19/ 23 [34]	20/ 35 [39]	19/ 43 [40]
10^{-4}	16/ 20 [28]	15/ 28 [28]	18/ 37 [37]	19/ 43 [40]
10^{-5}	15/ 20 [26]	14/ 27 [26]	17/ 37 [35]	19/ 43 [40]
10^{-6}	16/ 21 [28]	14/ 27 [26]	17/ 37 [34]	19/ 43 [40]
10^{-7}	16/ 21 [28]	14/ 27 [26]	17/ 37 [35]	19/ 43 [40]
10^{-8}	16/ 22 [28]	14/ 27 [26]	17/ 37 [35]	19/ 43 [41]

$\varepsilon \setminus$ TOL	10^{-1}	10^{-2}	10^{-3}	10^{-4}
10^{-2}	diverg.	40⋆/ 24 [353]	40⋆/ 43 [435]	40⋆/ 69 [547]
10^{-3}	40⋆/ 10 [297]	26/ 44 [286]	21/ 75 [305]	18/ 99 [326]
10^{-4}	40⋆/ 21 [352]	17/ 70 [243]	16/ 92 [275]	15/ 114 [304]
10^{-5}	35/ 33 [354]	15/ 70 [219]	14/ 93 [243]	14/ 115 [286]
10^{-6}	33/ 37 [348]	15/ 70 [220]	14/ 93 [244]	14/ 115 [296]
10^{-7}	40⋆/ 34 [411]	29/ 79 [461]	29/ 88 [495]	18/ 104 [342]
10^{-8}	40⋆/ 32 [403]	40⋆/ 50 [483]	31/ 89 [525]	32/ 115 [656]

$\varepsilon \setminus$ TOL	10^{-1}	10^{-2}	10^{-3}	10^{-4}
10^{-2}	diverg.	diverg.	40⋆/ 86 [3047]	40⋆/ 158 [5078]
10^{-3}	diverg.	40⋆/ 70 [2726]	40⋆/ 119 [4015]	37/ 214 [6100]
10^{-4}	31/ 63 [2113]	40⋆/ 78 [3050]	20/ 263 [4055]	20/ 431 [6486]
10^{-5}	40⋆/ 82 [3060]	16/ 208 [2721]	19/ 294 [4380]	18/ 454 [6198]
10^{-6}	40⋆/ 82 [3087]	16/ 214 [2733]	19/ 296 [4435]	18/ 454 [6314]
10^{-7}	21/ 86 [1831]	18/ 205 [3058]	19/ 296 [4532]	18/ 455 [6472]
10^{-8}	diverg.	diverg.	diverg.	diverg.

$\varepsilon \setminus$ TOL	10^{-1}	10^{-2}	10^{-3}	10^{-4}
10^{-2}	40⋆/ 13 [5997]	40⋆/ 68 [12117]	40⋆/ 239 [35923]	40⋆/678 [119583]
10^{-3}	40⋆/ 32 [8081]	40⋆/179 [28095]	40⋆/ 334 [44798]	40⋆/ 661 [86097]
10^{-4}	40⋆/ 71 [13974]	33/ 368 [45204]	24/ 795 [70727]	18/1429 [82560]
10^{-5}	40⋆/ 90 [14493]	37/ 476 [59433]	18/1162 [77307]	17/1818 [112571]
10^{-6}	40⋆/902 [133602]	31/1250 [127105]	37/1387 [132800]	35/1798 [169726]
10^{-7}	†	†	†	†
10^{-8}	†	†	†	†

Table 8. Direct comparison of the results for the discrete Newton approach with the Q_2/P_1 Stokes element for $\alpha = 0.9$; the parameters ε and TOL as step-length parameter, resp., as stopping criterion are varied. The results are shown for grid refinement level 2 (top) up to level 5 (bottom). We always provide the total number of nonlinear iterations (#NN), the averaged number of linear sweeps (#NL) per Newton step and the elapsed CPU time in seconds (in brackets). The maximum number of nonlinear Newton steps is 40 († - maximum CPU time exceeded).

The results clearly indicate that the right choice of the step-length parameter ε might be a delicate task: Choosing ε too big, then the advantageous quasi-quadratic convergence behavior may get lost, while very small parameter values for ε can lead to divergence, due to numerical instabilities. Additionally, the range of 'good' parameter values ε may also depend on the mesh width h and much more significantly on the nonlinearity of the problem, which is determined in our case via the parameter α; being outside of the range of admissible values, the increase in necessary CPU time can be extremely big.

	$\alpha = 0.5$		$\alpha = 0.9$	
Level	#NN/#NL	CPU	#NN/#NL	CPU
2	6/27	11	17/37	35
3	8/65	109	14/93	243
4	8/140	941	19/294	4380
5	9/723	22105	18/1162	77307

Table 9. Summarized presentation of the results for the discrete Newton approach with the Q_2/P_1 Stokes element for $\alpha = 0.5$ and $\alpha = 0.9$ on the different mesh levels. The calculations are performed for our 'preferred' configuration $\varepsilon = 10^{-5}$ and $TOL = 10^{-3}$ which seems to give the most robust convergence behavior.

Additionally, we analyze the influence of the prescribed tolerance parameter TOL which determines the relative accuracy for solving the linear subproblems. Here, the consequences are not so dramatic: Choosing 'big' values for TOL might destroy the quadratic nonlinear convergence properties, while very small parameters will not further improve the global nonlinear convergence behavior. However, this 'non-optimal' choice can significantly increase the total CPU time such that the recommendation is to gain between 2 - 4 digits of relative defect improvement in each nonlinear iteration as stopping criterion for the linear problems.

7 Conclusion

In this comparative study, we analyzed the influence of two different FEM discretization techniques (conforming Q_2/P_1, nonconforming $\tilde{Q}_1/Q_0$ elements) and solution procedures (nonlinear Newton variants, multigrid and Krylov-space solvers for the linear subproblems) onto the approximation properties and particularly the total efficiency of corresponding simulation tools for incompressible fluids. We discussed algorithmic details and provided numerical results for laminar steady-state flow examples including Newtonian and non-Newtonian behavior of *power law* type.

The following two approaches have been compared which both are quite popular in the CFD community; additionally, both of them are representative for typical methodologies which are in use for such types of flow simulations:

1. The Q_2/P_1 Stokes element with central differencing for the convective term and with a discrete nonlinear Newton solver based on 'divided differences' together with a preconditioned single-grid GMRES method for the auxiliary linear problems of Oseen type:

This pair of FEM functions leads due to the involved biquadratic polynomials to a higher order of accuracy than compared with linear approaches, at least for the considered low up to medium Re numbers; in contrast, for higher Re numbers, the question of stabilizing the discretized convective terms in the FEM context while maintaining the higher order accuracy has not been discussed and is one of the current research topics in the mathematical CFD community.

While the discrete Newton method leads in most cases - up to the question of stabilizing the 'divided differences' approach - to quite satisfying results concerning the numerical stability and efficiency, the involved GMRES solver as prototype for a non-multigrid Krylov-space method shows the expected dependence on mesh size which leads to huge numbers of linear iteration steps if the mesh width has to be decreased by accuracy reasons.

2. The nonconforming rotated bilinear $\tilde{Q}_1/Q_0$ Stokes element with upwinding resp. streamline-diffusion stabilization for the convective term and with a continuous nonlinear Newton solver together with an adapted multigrid method for the resulting Oseen-type subproblems:

The resulting accuracy of this 'linear' approach is lower such that up to 5 - 10 times more grid points are needed to produce results of similar quality as with the Q_2/P_1 approach. However, highly sophisticated FEM discretization techniques for the convective terms are available which can be directly applied for convection-dominated flows while maintaining a similar accuracy and robustness as for the considered low Re number flow configurations.

The advantage of this approach is - besides the continuous Newton solver for the nonlinearity which however can be performed for the Q_2/P_1 scheme, too - the already realized multigrid solver for the linearized problems. After a careful optimization of all multigrid components in relation to the underlying FEM spaces, the typical robust and very efficient convergence behavior of multigrid approaches can be obtained such that the linear problems are solved with a numerical efficiency which is more or less independent of the problem size, the mesh topology and also the type of problems, as for instance Stokes or Oseen equations for different Re numbers, coming from Newtonian and non-Newtonian models.

Concerning the question of the 'total efficiency', that means the amount of CPU seconds to provide a certain accuracy for a given flow problem, the

answer due to our massive test calculations should be as follows: the higher order Q_2/P_1 approach requires significantly less grid points, however due to the missing multigrid solvers, the corresponding CPU time is huge. Altogether, the simpler nonconforming $\tilde{Q}_1/Q_0$ Stokes element together with the already realized multigrid components seems to be the better compromise at the moment, if we analyze the available flexibility and efficiency of this combination: 'Multigrid is a must for incompressible flow problems!'

As an outlook, it is clear that the examined Q_2/P_1 approach shows a huge potential for future improvement for complex fluid simulations, but the potentially higher order approximation properties have to be combined with adequate multigrid solvers. This must be one of the main tasks for Mathematics and Numerics in the CFD community and will be one of the major future research topics. Realizing the vision of a 'robust and flexible higher order FEM discretization' with 'accurate FEM treatment of the convective terms' together with 'adaptive local grid refinement' on the basis of 'rigorous a posteriori error control mechanisms for user-specified functionals' in combination with 'efficient nonlinear Newton-like and linear multigrid-like solvers', that should be the aim for future work!

Bibliography

[1] J. Baranger and K. Najib. Analyse numerique des écoulements quasi-newtoniens dont la viscosity obeit la loi puissance ou la loi de carreau. *Numer. Math.*, 58:35–49, 1990.

[2] R. Bramley and X. Wang. *SPLIB: A library of iterative methods for sparse linear systems*. Department of Computer Science, Indiana University, Bloomington, IN, 1997. `http://www.cs.indiana.edu/ftp/bramley/splib.tar.gz`.

[3] C. S. Brenner. Korn's inequalities for piecewise H^1 vector fields. *IMI Preprint Series*, 5:1–21, 2002.

[4] P. Hansbo and M. G. Larson. A simple nonconforming bilinear element for the elasticity problem. In *CIMNE*, Barcelona, Spain, 2001.

[5] J. Hron, J. Málek, J. Nečas, and K. R. Rajagopal. Numerical simulations and global existence of solutions of two dimensional flows of fluids with pressure and shear dependent viscosities. *Math. Comp. Sim.*, 2002. to appear.

[6] D. Kuzmin, M. Möller, and S. Turek. Multidimensional fem-fct schemes for arbitrary time-stepping. *J. Comp. Phys.*, 2002. (to appear).

[7] A. Ouazzi, R. Schmachtel, and S. Turek. Multigrid methods for stabilized nonconforming finite elements for incompressible flow involving the deformation tensor formulation. *J. Numer. Math.*, 10:235–248, 2002.

[8] A. Prohl and M. Růžička. On fully implicit space-time discretization for motions of incompressible fluids with shear-dependent viscosity: the case $p \leq 2$. *SIAM J. Numer. Anal.*, 39:214–249, 2001.

[9] R. Rannacher and S. Turek. A simple nonconforming quadrilateral stokes element. *Numer. Meth. Part. Diff. Equ.*, 8:97–111, 1992.

[10] Y. Saad and M. H. Schultz. GMRES: A generalized minimal residual algorithm for solving nonsymmetric linear systems. *SIAM J. Sci. Stat. Comput.*, 7:856–869, 1986.

[11] D. Schaeffer. Instability in the evolution equations describing incompressible granular flow. *J. Diff. Eq.*, 66:19–50, 1987.

[12] M. Schäfer and S. Turek. Benchmark computations of laminar flow around cylinder. In E.H. Hirschel, editor, *Flow Simulation with High-Performance Computers II*, volume 52 of *Notes on Numerical Fluid Mechanics*, pages 547–566. Vieweg, 1996.

[13] R. Schmachtel. *Robuste lineare und nichtlineare Lösungsverfahren für die inkompressiblen Navier-Stokes-Gleichungen*. PhD thesis, University of Dortmund, 2002. (to be published).

[14] S. Turek. *Efficient solvers for incompressible flow problems: An algorithmic and computational approach*, volume 6 of *LNCSE*. Springer, Berlin, 1999.

[15] S. Turek et al. **FEATFLOW** – *Finite element software for the incompressible Navier-Stokes equations: User Manual, Release 1.2*, 1999. `http://www.featflow.de`.

[16] S. Turek and S. Kilian. *The Virtual Album of Fluid Motion*. Multimedia DVD. Springer, 2002. `http://www.featflow.de/album`.

[17] H. A. van der Vorst. Bi-CGSTAB: A fast and smoothly converging variant of Bi-CG for the solution of nonsymmetric linear systems. *SIAM J. Sci. Stat. Comput.*, 13(2):631–644, 1992.

[18] S. P. Vanka. Implicit multigrid solutions of navier-stokes equations in primitive variables. *J. Comp. Phys.*, 65:138–158, 1985.